Materials Physics and Mechanics. 2022;50(2): 319-330
Research article
http://dx.doi.org/10.18149/MPM.5022022_11

Submitted: April 11, 2022
Approved: August 5, 2022
Accepted: October 18, 2022

Finite element algorithm for implementing variants of physically nonlinear defining equations in the calculation of an ellipsoidal shell

A.Sh. Dzhabrailov[1]✉, A.P. Nikolaev[1], Yu.V. Klochkov[1], N.A. Gureyeva[2]

[1]FGBOU VPO Volgograd state agrarian University, 400002, Volgograd, PR. University, d. 26, Russia

Financial University under the Government of the Russian Federation, Moscow, Russia

✉ arsen82@yandex.ru

Abstract. The defining equations at the loading step are obtained in three variants. In the first variant, the relations between strain increments and stress increments are obtained by differentiating the equations of the theory of small elastic-plastic deformations using the hypothesis of plastic incompressibility of the material. In the second variant, the assumption of plastic incompressibility was not used. The relations between the first invariants of stress and strain tensors were considered to be known from the extension test. In the third variant, the defining equations at the loading step are obtained without dividing the strain increments into elastic and plastic parts based on the hypothesis of proportionality of the components of the strain increment deviators and the components of the stress increment deviators using the relations between the first invariants of the stress and strain increment tensors determined experimentally. The numerical example shows the preference of the third variant of the defining equations.

Keywords: shell, strain tensor, finite element, displacement vector, physical nonlinearity, plasticity matrix, stress tensor

Acknowledgements*. No external funding was received for this study.*

Citation: Dzhabrailov ASh, Nikolaev AP, Klochkov YuV, Gureyeva NA. Finite element algorithm for implementing variants of physically nonlinear defining equations in the calculation of an ellipsoidal shell. *Materials Physics and Mechanics*. 2022;50(2): 319-330. DOI: 10.18149/MPM.5022022_11.

1. Introduction

At present, the theory of shells has a fairly complete outline [1,2,3,4]. Obtaining analytical solutions for the vast majority of problems in engineering practice is not possible due to the complexity of the equations. Therefore, the development and improvement of numerical methods for strength calculations of engineering structures is an urgent task at the present time. One of the priority directions of the world's leading researchers in the field of studying thin-walled shell structures is taking into account the physical nonlinearity of the material used [5-15]. The most effective among modern methods used in the design of thin-walled structures is the finite element method (FEM). The development of the FEM is devoted to the works of many domestic and foreign authors [16-25]. When taking into account the physical nonlinearity, the above-mentioned works use the classical assumption of the invariance of the

volume as a result of elastic-plastic deformations, which does not quite correspond to the physical meaning of the deformation process and in some cases can lead to significant errors. Moreover, in physically nonlinear calculations, it is customary to divide the strain increments at the loading step into elastic and plastic parts. In the presented work, using the assumption that the components of the deviators of the increments of strains are proportional to the components of the deviators of the increments of stresses, the authors obtained new constitutive equations in which the above separation of strains at the loading step is absent.

2. Materials and methods

Basic relations. The position of the point M^0 of the middle surface of the ellipsoid is determined by the radius vector [26]

$$\mathbf{R^0} = asinT\mathbf{i} + bcosTsint\mathbf{j} + ccosTcost\mathbf{k}, \quad (1)$$

where a,b,c – segments cut off on the OX, OY, OZ axes; $\mathbf{i},\mathbf{j},\mathbf{k}$ – orts the Cartesian coordinate system; T – ellipse parameter in the OZ plane; t – ellipse parameter in the plane perpendicular to the OX axis.

The basis vectors at the point M^0 can be found as follows (1):

$$\mathbf{a}_1^0 = \mathbf{R}_{,T}^{\mathbf{0}} = acosT\mathbf{i} - bsinTsint\mathbf{j} - csinTcost\mathbf{k}; \quad (2)$$
$$\mathbf{a}_2^0 = \mathbf{R}_{,t}^{\mathbf{0}} = bcosTcost\mathbf{j} - ccosTsint\mathbf{k}.$$

The normal to the middle surface is determined by the vector product:

$$\mathbf{a}_3^0 = \frac{\mathbf{a}_1^0 \times \mathbf{a}_2^0}{|\mathbf{a}_1^0 \times \mathbf{a}_2^0|} = \frac{u_1}{u}\mathbf{i} + \frac{u_2}{u}\mathbf{j} + \frac{u_3}{u}\mathbf{k}, \quad (3)$$

where $u_1 = bcsinTcosT$; $u_2 = acsintcos^2T$; $u_3 = abcostcos^2T$; $u = \sqrt{u_1^2 + u_2^2 + u_3^2}$.

Dependencies (2) and (3) are presented in the following form:

$$\underset{3\times1}{\{\mathbf{a}^0\}} = \underset{3\times3}{[\tau(T,t)]}\underset{3\times1}{\{\mathbf{i}\}};\ \underset{3\times1}{\{\mathbf{i}\}} = \underset{3\times3}{[\tau(T,t)]^{-1}}\underset{3\times1}{\{\mathbf{a}^0\}}, \quad (4)$$

where $\underset{1\times3}{\{\mathbf{a}^0\}^T} = \{\mathbf{a}_1^0\mathbf{a}_2^0\mathbf{a}_3^0\}$; $\underset{1\times3}{\{\mathbf{i}\}^T} = \{\mathbf{ijk}\}$.

Differentiating the basis vectors (4) of an arbitrary point of the middle surface, we express them by the components of the same basis:

$$\underset{3\times1}{\{\mathbf{a}^0{}_{,T}\}} = \underset{3\times3}{[\tau(T,t)_{,T}]}\underset{3\times1}{\{\mathbf{i}\}} = \underset{3\times3}{[\tau(T,t)_{,T}]}\underset{3\times3}{[\tau(T,t)]^{-1}}\underset{3\times1}{\{\mathbf{a}^0\}} = \underset{3\times3}{[M]}\underset{3\times1}{\{\mathbf{a}^0\}};$$
$$\underset{3\times1}{\{\mathbf{a}^0{}_{,t}\}} = \underset{3\times3}{[\tau(T,t)_{,t}]}\underset{3\times1}{\{\mathbf{i}\}} = \underset{3\times3}{[\tau(T,t)_{,t}]}\underset{3\times3}{[\tau(T,t)]^{-1}}\underset{3\times1}{\{\mathbf{a}^0\}} = \underset{3\times3}{[N]}\underset{3\times1}{\{\mathbf{a}^0\}}, \quad (5)$$

where $\underset{1\times3}{\{\mathbf{a}^0{}_{,T}\}^T} = \{\boldsymbol{a}_{1,T}^0\boldsymbol{a}_{2,T}^0\boldsymbol{a}_{3,T}^0\}$; $\underset{1\times3}{\{\mathbf{a}^0{}_{,t}\}^T} = \{\boldsymbol{a}_{1,t}^0\boldsymbol{a}_{2,t}^0\boldsymbol{a}_{3,t}^0\}$.

Consider several main positions of the points of the middle surface of the shell during deformation: the deformed position after (j-1) loading steps (point M, displacement vector $\mathbf{v}$) and the position after the j^{th} loading step (point M^*, displacement vector $\Delta\mathbf{v}$). The points of an arbitrary layer of the shell, spaced at a distance of ξ from the median line, are denoted by the symbols $M^{0\xi}$, M^{ξ}, and $M^{*\xi}$ corresponding to the indicated states.

Radius vectors of the points M, M^*, $M^{0\xi}$, M^{ξ}, and $M^{*\xi}$ are determined as follows:

$$\mathbf{R^{0\xi}}=\mathbf{R}^0+\xi\mathbf{a_3^0};\ \mathbf{R}=\mathbf{R}^0+\mathbf{v};\ \mathbf{R}^*=\mathbf{R}+\Delta\mathbf{v}; \quad (6)$$
$$\mathbf{R}^{\xi}=\mathbf{R^{0\xi}}+\mathbf{v}+\xi(\mathbf{a}_3-\mathbf{a}_3^{\mathbf{0}});\ \mathbf{R}^{*\xi}=\mathbf{R}^{\xi}+\Delta\mathbf{v}+\xi(\mathbf{a}_3^*-\mathbf{a}_3),$$

where $\mathbf{a}_3$ and $\mathbf{a}_3^*$ – normalized vectors to the middle surface of the shell at the points M and M^*.

The components of the displacement vectors $\mathbf{v}$ and $\Delta\mathbf{v}$ included in (6) are determined on the initial basis of the point M^0:

$$\mathbf{v} = v^i\mathbf{a}_i^0;\ \Delta\mathbf{v} = \Delta v^i\mathbf{a}_i^0. \quad (7)$$

The basis vectors at the points $M^{0\xi}$, M^{ξ}, and $M^{*\xi}$ are found by differentiating (6) and taking into account (5):

$$\mathbf{g}_1^0 = \mathbf{R}_{,T}^{0\xi};\ \mathbf{g}_1 = \mathbf{R}_{,T}^{\xi} + \mathbf{v}_{,T} + \xi(\mathbf{a}_{3,T} - \mathbf{a}_{3,T}^0);$$

$$\mathbf{g}_1^* = \mathbf{R}_{,T}^* = \mathbf{g}_1 + \Delta\mathbf{v}_{,T} + \xi\left(\boldsymbol{a}_{3,T}^* - \boldsymbol{a}_{3,T}\right); \quad (8)$$
$$\mathbf{g}_2^0 = \mathbf{R}_{,t}^{0\xi}; \mathbf{g}_2 = \mathbf{R}_{,t}^{\xi} + \mathbf{v}_{,t} + \xi\left(\mathbf{a}_{3,t} - \mathbf{a}_{3,t}^0\right);$$
$$\mathbf{g}_2^* = \mathbf{R}_{,t}^* = \mathbf{g}_2 + \Delta\mathbf{v}_{,t} + \xi\left(\boldsymbol{a}_{3,t}^* - \boldsymbol{a}_{3,t}\right).$$

The derivatives of the vectors **v** and **Δv** can be obtained by differentiating (7) and taking into account (5):

$$\mathbf{v}_{,\alpha} = z_\alpha^m \mathbf{a}_m^0; \mathbf{v}_{,\alpha\beta} = z_{\alpha\beta}^m \mathbf{a}_m^0$$
$$\Delta\mathbf{v}_{,\alpha} = f_\alpha^m \mathbf{a}_m^0; \Delta\mathbf{v}_{,\alpha\beta} = f_{\alpha\beta}^m \mathbf{a}_m^0, \quad (9)$$

where z_α^m and $z_{\alpha\beta}^m$ – functions of the displacement vector components **v** and their derivatives; f_α^m, $f_{\alpha\beta}^m$ – functions of the displacement vector components **Δv** and their derivatives; for α=1 we understand the derivative with respect to the parameter *T*; for α=2 – differentiation with respect to the parameter *t*.

The unit normal vectors at the points M and M^* can be represented by the vector products of the corresponding basis vectors tangent to the middle surface of the ellipsoid at the points under consideration. When calculating in a geometrically linear formulation, these unit vectors can be represented by the expressions:

$$\mathbf{a}_3 = \frac{\mathbf{a}_1 \times \mathbf{a}_2}{\sqrt{a}}; \mathbf{a}_3^* = \frac{\mathbf{a}_1^* \times \mathbf{a}_2^*}{\sqrt{a}}, \quad (10)$$

where $\mathbf{a}_1 = (\mathbf{R}^0 + \mathbf{v})_{,T}$; $\mathbf{a}_2 = (\mathbf{R}^0 + \mathbf{v})_{,t}$; $\mathbf{a}_1^* = (\mathbf{R} + \mathbf{\Delta v})_{,T}$; $\mathbf{a}_2^* = (\mathbf{R} + \mathbf{\Delta v})_{,t}$; $a = a_{11}a_{22} - a_{12}a_{21}$ – determinant of the metric tensor at a point M.

When determining the curvature in an arbitrary shell layer spaced at a distance ξ from the median line, one can apply the equations of continuum mechanics [27]:

$$\varepsilon_{\alpha\beta}^{\xi} = \frac{1}{2}\left(g_{\alpha\beta} - g_{\alpha\beta}^0\right); \Delta\varepsilon_{\alpha\beta}^{\xi} = \frac{1}{2}\left(g_{\alpha\beta}^* - g_{\alpha\beta}\right), \quad (11)$$

where $g_{\alpha\beta}^0 = \mathbf{g}_\alpha^0 \mathbf{g}_\beta^0; g_{\alpha\beta} = \mathbf{g}_\alpha \mathbf{g}_\beta; g_{\alpha\beta}^* = \mathbf{g}_\alpha^* \mathbf{g}_\beta^*$ – covariant components of metric tensors at corresponding points.

When using (8), (9), and (10), the deformations at an arbitrary point of the shell (11) are represented by the expressions:

$$\varepsilon_{\alpha\beta}^{\xi} = \varepsilon_{\alpha\beta} + \xi\chi_{\alpha\beta}; \Delta\varepsilon_{\alpha\beta}^{\xi} = \Delta\varepsilon_{\alpha\beta} + \xi\Delta\chi_{\alpha\beta}, \quad (12)$$

where $\varepsilon_{\alpha\beta}^{\xi}$, $\chi_{\alpha\beta}$ – deformation and curvature of the middle surface of the shell at the point M; $\Delta\varepsilon_{\alpha\beta}$, $\Delta\chi_{\alpha\beta}$ – increments of deformations and curvature of the middle surface at a point M^*.

At the loading step, the deformation parameters of the middle surface in a linear formulation are determined by the expressions:

$$\Delta\varepsilon_{\alpha\beta} = \frac{1}{2}\left(\mathbf{a}_\alpha^0 \Delta\mathbf{v}_{,\beta} + \mathbf{a}_\beta^0 \Delta\mathbf{v}_{,\alpha}\right); \quad (13)$$
$$\Delta\chi_{\alpha\beta} = \frac{1}{2}\left(\mathbf{a}_\alpha^0 \Delta\mathbf{v}_{,\beta} + \mathbf{a}_\beta^0 \Delta\mathbf{v}_{,\alpha} + \mathbf{a}_\alpha^0(\mathbf{a}_3^* - \mathbf{a}_3)_{,\beta} + \mathbf{a}_\beta^0(\mathbf{a}_3^* - \mathbf{a}_3)_{,\alpha}\right).$$

Expressions (12) and (13) taking into account (8), (9) and (10) are presented in matrix form:

$$\underset{3\times1}{\left\{\varepsilon^{\xi}\right\}} = \underset{3\times6}{[G]}\underset{6\times1}{\{\varepsilon\}} = \underset{3\times6}{[G]}\underset{6\times3}{[L]}\underset{3\times1}{\{v\}}; \underset{3\times1}{\left\{\Delta\varepsilon^{\xi}\right\}} = \underset{3\times6}{[G]}\underset{6\times1}{\{\Delta\varepsilon\}} = \underset{3\times6}{[G]}\underset{6\times3}{[L]}\underset{3\times1}{\{\Delta v\}}, \quad (14)$$

where $\left\{\varepsilon^{\xi}\right\}^T = \left\{\varepsilon_{11}^{\xi}\varepsilon_{22}^{\xi}2\varepsilon_{12}^{\xi}\right\}$; $\left\{\Delta\varepsilon^{\xi}\right\}^T = \left\{\Delta\varepsilon_{11}^{\xi}\Delta\varepsilon_{22}^{\xi}2\Delta\varepsilon_{12}^{\xi}\right\}$;

$\{\varepsilon\}^T = \{\varepsilon_{11}; \varepsilon_{22}; 2\varepsilon_{12}; \chi_{11}; \chi_{22}; 2\chi_{12}\}; \{v\}^T = \{v^1; v^2; v^3\}$;

$\{\Delta v\}^T = \{\Delta v^1; \Delta v^2; \Delta v^3\}; \{\Delta\varepsilon\}^T = \{\Delta\varepsilon_{11}; \Delta\varepsilon_{22}; 2\Delta\varepsilon_{12}; \Delta\chi_{11}; \Delta\chi_{22}; 2\Delta\chi_{12}\}$;

$[L]$ – transformation matrix.

Discretization element at the loading step. An arbitrary quadrangular fragment of the middle surface of the shell with nodes *i*, *j*, *k*, and *l* is taken as a finite element. To perform the numerical integration procedure, this fragment is approximated by a square with local coordinates ζ and η, varying within $-1 \le \zeta,\eta \le 1$. The mapping is implemented using bilinear functions:

$$\lambda = \underset{1\times4}{\{f(\zeta,\eta)\}^T}\underset{4\times1}{\{\lambda_y\}}, \quad (15)$$

where $\{\lambda_y\}^T = \{\lambda^i\lambda^j\lambda^k\lambda^l\}$, and the symbol λ means the values of the nodal parameters *T* and *t*, which are further denoted by the symbols θ^1 and θ^2, respectively.

After the derivatives (15) are found, the coordinates θ^α in the system $\zeta,\eta(\theta,^{\alpha}_{\zeta}, \theta,^{\alpha}_{\eta})$ and local coordinates ζ,η are differentiated with respect to the global unknowns θ^α $(\zeta,_\alpha,\eta,_\alpha,\zeta,_{\alpha\beta},\eta,_{\alpha\beta})$.

As nodal variable parameters for (*j*-1) previous steps, the components of the displacement vector and their derivatives in local and global coordinate systems are selected:

$$\underset{1\times12}{\{v_l^n\}^T} = \left\{v^{ni}v^{nj}v^{nk}v^{nl}v,^{ni}_{\zeta}\, v,^{nj}_{\zeta}\, v,^{nk}_{\zeta}\, v,^{nl}_{\zeta}\, v,^{ni}_{\eta}\, v,^{nj}_{\eta}\, v,^{nk}_{\eta}\, v,^{nl}_{\eta}\right\}; \quad (16)$$

$$\underset{1\times12}{\{v_g^n\}^T} = \{v^{ni}v^{nj}v^{nk}v^{nl}v,^{ni}_{\theta^1}\, v,^{nj}_{\theta^1}\, v,^{nk}_{\theta^1}\, v,^{nl}_{\theta^1}\, v,^{ni}_{\theta^2}\, v,^{nj}_{\theta^2}\, v,^{nk}_{\theta^2}\, v,^{nl}_{\theta^2}\},$$

where *n*=1,2,3.

Similarly, at the j^{th} loading step

$$\underset{1\times12}{\{\Delta v_l^n\}^T} = \left\{\Delta v^{ni}\Delta v^{nj}\Delta v^{nk}\Delta v^{nl}\Delta v,^{ni}_{\zeta}\, \Delta v,^{nj}_{\zeta}\, \Delta v,^{nk}_{\zeta} \ldots\ldots \Delta v,^{nk}_{\eta}\, \Delta v,^{nl}_{\eta}\right\}; \quad (17)$$

$$\underset{1\times12}{\{\Delta v_g^n\}^T} = \{\Delta v^{ni}\Delta v^{nj}\Delta v^{nk}\Delta v^{nl}\Delta v,^{ni}_{\theta^1} \ldots\ldots \Delta v,^{nj}_{\theta^2}\, \Delta v,^{nk}_{\theta^2}\, \Delta v,^{nl}_{\theta^2}\}.$$

The local basis nodal vectors of the finite element (FE) at the loading step can be represented as:

$$\underset{1\times36}{\{\Delta V_y^l\}^T} = \left\{\underset{1\times12}{\{\Delta v^{1l}\}^T}\underset{1\times12}{\{\Delta v^{2l}\}^T}\underset{1\times12}{\{\Delta v^{3l}\}^T}\right\}; \underset{1\times36}{\{\Delta V_y^g\}^T} = \left\{\underset{1\times12}{\{\Delta v^{1g}\}^T}\underset{1\times12}{\{\Delta v^{2g}\}^T}\underset{1\times12}{\{\Delta v^{3g}\}^T}\right\}. \quad (18)$$

When using differential dependencies

$$v,^n_{\zeta} = v,^n_{\theta^1}\,\theta,^1_{\zeta} + v,^n_{\theta^2}\,\theta,^2_{\zeta}; v,^n_{\eta} = v,^n_{\theta^1}\,\theta,^1_{\eta} + v,^n_{\theta^2}\,\theta,^2_{\eta}\,; (n = 1,2,3) \quad (19)$$

between nodal unknowns in local and global coordinate systems, the following matrix relation takes place:

$$\underset{36\times1}{\{\Delta V_y^l\}} = \underset{36\times36}{[H]}\,\underset{36\times1}{\{\Delta V_y^g\}}. \quad (20)$$

As a result of deformation, the position of the internal point of the FE can be determined through the nodal unknowns using the expressions:

$$v^n = \underset{1\times12}{\{\varphi\}^T}\underset{12\times1}{\{v^{nl}\}}; \Delta v^n = \underset{1\times12}{\{\varphi\}^T}\underset{12\times1}{\{\Delta v^{nl}\}}; \quad n = 1,2,3, \quad (21)$$

where the structure $\{\varphi\}^T$ includes Hermite polynomials of the third degree [28].

Based on (14), increments of step strain, taking into account (21), will take the form:

$$\underset{3\times1}{\{\Delta\varepsilon^\xi\}} = \underset{3\times66}{[G]}\underset{3\times3}{[L]}\underset{3\times1}{\{\Delta v\}} = \underset{3\times66}{[G]}\underset{3\times33}{[L]}\,\underset{36\times1}{[A]\{\Delta V_y^l\}} = \underset{3\times66}{[G]}\,\underset{36\times36}{[B]}\underset{36\times1}{\{\Delta V_y^l\}}, \quad (22)$$

where $\underset{3\times36}{[\mathrm{A}]} = \begin{bmatrix} \underset{1\times12}{\{\varphi\}^T} & \underset{1\times12}{\{0\}^T} & \underset{1\times12}{\{0\}^T} \\ \underset{1\times12}{\{0\}^T} & \underset{1\times12}{\{\varphi\}^T} & \underset{1\times12}{\{0\}^T} \\ \underset{1\times12}{\{0\}^T} & \underset{1\times12}{\{0\}^T} & \underset{1\times12}{\{\varphi\}^T} \end{bmatrix}$.

Relationships between strain increments and stress increments at the loading step. The constitutive equations of the theory of small elastoplastic deformations in a curvilinear coordinate system are written as [29]:

$$\varepsilon^\xi_{\alpha\beta} - \frac{1}{3}g_{\alpha\beta}P^\xi_\varepsilon = \frac{3}{2}\frac{\varepsilon_i}{\sigma_i}\left(\sigma_{\alpha\beta} - \frac{1}{3}g_{\alpha\beta}P_\sigma\right), \quad (23)$$

where $\varepsilon^\xi_{\alpha\beta}$ – covariant strain tensor components; $P^\xi_\varepsilon = \varepsilon^\xi_{\alpha\beta}g^{\alpha\beta}$ – the first invariant of the strain tensor; $g_{\alpha\beta}, g^{\alpha\beta}$ – covariant and contravariant components of the metric tensor; $\sigma_{\alpha\beta}$ –

covariant stress tensor components; $P_\sigma = \sigma_{\alpha\beta} g^{\alpha\beta}$ – the first invariant of the stress tensor; ε_i – strain intensity; σ_i – stress intensity.

The dependence between the first invariants of the strain and stress tensor, taking into account the hypothesis of the incompressibility of the material, is written as [30]:

$$P_\varepsilon^\xi = \frac{1-2\mu}{E} P_\sigma = K_1 P_\sigma, \quad (24)$$

where μ – the transverse strain coefficient; E – elasticity modulus of the material.

If we disregard the hypothesis about the incompressibility of the material, then relation (24) can be represented as follows:

$$P_\varepsilon^\xi = K_2 P_\sigma = \frac{3}{2}\frac{(1-2\mu)}{(1+\mu)}\frac{1}{E_{sd}} P_\sigma, \quad (25)$$

where the coefficient K_2 is determined on the basis of experience with a simple tension of the rod; E_{sd} – secant modulus of the deformation diagram.

Taking into account (24) and (25) dependences (23) can be rewritten as:

$$\varepsilon_{\alpha\beta}^\xi = \frac{3}{2}\frac{\varepsilon_i}{\sigma_i}\sigma_{\alpha\beta} + \frac{1}{3} g_{\alpha\beta} P_\sigma \left(-\frac{3}{2}\frac{\varepsilon_i}{\sigma_i} + K_m\right), \quad (26)$$

where $m = 1, 2$.

Dependences between strain increments and stress increments at the loading step are determined by differentiation of (26):

$$\Delta\varepsilon_{\alpha\beta}^\xi = \frac{\partial \varepsilon_{\alpha\beta}^\xi}{\partial \sigma_{11}}\Delta\sigma_{11} + \frac{\partial \varepsilon_{\alpha\beta}^\xi}{\partial \sigma_{22}}\Delta\sigma_{22} + \frac{\partial \varepsilon_{\alpha\beta}^\xi}{\partial \sigma_{12}}\Delta\sigma_{12}, \quad (27)$$

where the coefficients K_m at the loading step are considered unchanged.

Based on (27), a matrix relation is formed:

$$\underset{3\times1}{\{\Delta\varepsilon^\xi\}} = \underset{3\times3}{[D_m]}\underset{3\times1}{\{\Delta\sigma_{\alpha\beta}\}}, \quad (28)$$

where $\{\Delta\sigma_{\alpha\beta}\}^T = \{\Delta\sigma_{11}\Delta\sigma_{22}\Delta\sigma_{12}\}$ – string of stress increments at the loading step; $m = 1, 2$ depending on the coefficient K_m used.

The author's version of the relationship between increments of strains and stresses suggests using the assumption that the components of the deviator of increments of strains are proportional to the components of the deviator of increments of stresses:

$$\Delta\varepsilon_{\alpha\beta}^\xi - \frac{1}{3} g_{\alpha\beta} P_{\Delta\varepsilon}^\xi = \frac{3}{2}\frac{{\varepsilon_i}^\Delta}{{\sigma_i}^\Delta}\left(\Delta\sigma_{\alpha\beta} - \frac{1}{3} g_{\alpha\beta} P_{\Delta\sigma}\right), \quad (29)$$

where $\Delta\varepsilon_{\alpha\beta}^\xi$ – covariant components of the strain increment tensor; $P_{\Delta\varepsilon}^\xi = \Delta\varepsilon_{\alpha\beta}^\xi g^{\alpha\beta}$ – the first invariant of the strain increment tensor; $\Delta\sigma_{\alpha\beta}$ – covariant components of the stress increment tensor; $P_{\Delta\sigma} = \Delta\sigma_{\alpha\beta} g^{\alpha\beta}$ – first invariant of the stress increment tensor; ${\varepsilon_i}^\Delta$ – intensity of strain increments; ${\sigma_i}^\Delta$ – intensity of stress increments.

In practical use in relations (29) it is assumed that the ratio of the intensities of strain increments and stress increments is equal to the ratio of increments of strain and stress intensities:

$$\frac{{\varepsilon_i}^\Delta}{{\sigma_i}^\Delta} = \frac{\Delta\varepsilon_i}{\Delta\sigma_i} = \frac{1}{E_x}, \quad (30)$$

where E_x – the chord modulus of the deformation diagram at the loading step.

Applying the tension-compression test to a rod, one can obtain relations between the first invariants of the tensors of strain increments and stress increments:

$$P_{\Delta\varepsilon} = K_3 P_{\Delta\sigma} = \frac{3}{2}\frac{(1-2\mu)}{(1+\mu)}\frac{1}{E_x}. \quad (31)$$

Taking into account (30) and (31) dependences (29) take the form:

$$\Delta\varepsilon_{\alpha\beta}^\xi = \frac{3}{2}\frac{1}{E_x}\Delta\sigma_{\alpha\beta} + \frac{1}{3} g_{\alpha\beta} P_{\Delta\sigma}\left(-\frac{3}{2}\frac{1}{E_x} + K_3\right). \quad (32)$$

Based on (32), a matrix relation is formed:

$$\underset{3\times1}{\{\Delta\varepsilon^{\xi}\}} = \underset{3\times3}{[D_3]}\underset{3\times1}{\{\Delta\sigma_{\alpha\beta}\}}. \quad (33)$$

Finite element stiffness matrix. When forming the stiffness matrix of the FE described above at the loading step, the principle of equality of the work of internal and external forces is used, which is determined by the expression

$$\Phi = \int_V \Delta\varepsilon^{\xi}_{\alpha\beta}\left(\sigma^{\alpha\beta} + \Delta\sigma^{\alpha\beta}\right) dV - \int_F \Delta v^i (P_i + \Delta P_i)\, dF, \quad (34)$$

where $\sigma^{\alpha\beta}$ and $\Delta\sigma^{\alpha\beta}$ – contravariant components of the stress tensor for (j-1) loading steps and the stress increment tensor at the j^{th} loading step; P_i and ΔP_i are covariant components of the vector of external loads.

Based on the ratios:

$$\Delta\sigma^{\alpha\beta} = g^{\alpha\rho} g^{\beta\tau} \Delta\sigma_{\rho\tau}$$

a matrix expression is compiled:

$$\underset{3\times1}{\{\sigma^{\alpha\beta}\}} = \underset{3\times3}{[g]}\underset{3\times1}{\{\Delta\sigma_{\alpha\beta}\}}. \quad (35)$$

To determine the stress increments in an arbitrary shell layer, using (28) and (33), one can obtain the matrix relation:

$$\underset{3\times1}{\{\Delta\sigma_{\alpha\beta}\}} = \underset{3\times3}{[D_m]^{-1}}\underset{3\times1}{\{\Delta\varepsilon^{\xi}\}}. \quad (36)$$

Taking into account (36) and (22), functional (34) can be written as:

$$\Phi = \underset{1\times36}{\{\Delta V_y^l\}^{\mathrm{T}}} \int_V \underset{36\times6}{[B]^T}\underset{6\times3}{[G]^{\mathrm{T}}}\underset{3\times3}{[g]}\underset{3\times1}{\{\sigma_{\alpha\beta}\}} dV + \underset{1\times36}{\{\Delta V_y^l\}^{\mathrm{T}}} \int_V \underset{36\times6}{[B]^T}\underset{6\times3}{[G]^{\mathrm{T}}}\underset{3\times3}{[D_m]^{-1}}\underset{3\times3}{[g]}\underset{3\times66\times36}{[G]\,[B]}\underset{36\times1}{\{\Delta V_y^l\}}\, dV -$$
$$\underset{1\times36}{\{\Delta V_y^l\}^{\mathrm{T}}} \int_F \underset{36\times3}{[A]^T}\underset{3\times1}{\{P\}} dF - \underset{1\times36}{\{\Delta V_y^l\}^{\mathrm{T}}} \int_F \underset{36\times3}{[A]^T}\underset{3\times1}{\{\Delta P\}} dF. \quad (37)$$

When using (20) and minimizing the functional (37) with respect to the nodal unknowns $\{\Delta V_y^g\}$, a matrix relation is formed:

$$\underset{36\times36}{[M]}\underset{36\times1}{\{\Delta V_y^g\}} = \underset{36\times1}{\{F\}} + \underset{36\times1}{\{f\}}, \quad (38)$$

where $\underset{36\times36}{[M]} = \underset{36\times36}{[H]^T} \int_V \underset{36\times6}{[B]^T}\underset{6\times3}{[G]^T}\underset{3\times3}{[D_m]^{-1}}\underset{3\times33\times66\times36}{[g][G]\,[B]}\, \mathrm{d}V\, \underset{36\times36}{[H]}$ – step stiffness matrix of a quadrangular FE; $\underset{36\times1}{\{F\}} = \underset{36\times36}{[H]^T} \int_F \underset{36\times3}{[A]^T}\underset{3\times1}{\{\Delta P\}} \mathrm{d}F$ – step vector of nodal loads; $\underset{36\times1}{\{f\}} = \underset{36\times36}{[H]^T} \int_F \underset{36\times3}{[A]^{\mathrm{T}}}\underset{3\times1}{\{P\}} dF - \underset{36\times36}{[H]^T} \int_V \underset{36\times6}{[B]^T}\underset{6\times3}{[G]^T}\underset{3\times3}{[g]}\underset{3\times1}{\{\sigma_{\alpha\beta}\}} dV$ – the Newton-Raphson residual.

3. Obtained results

In order to verify the proposed algorithms, the problem of calculating the strength of a fragment of an elliptical cylinder shown in Fig. 1 was solved.

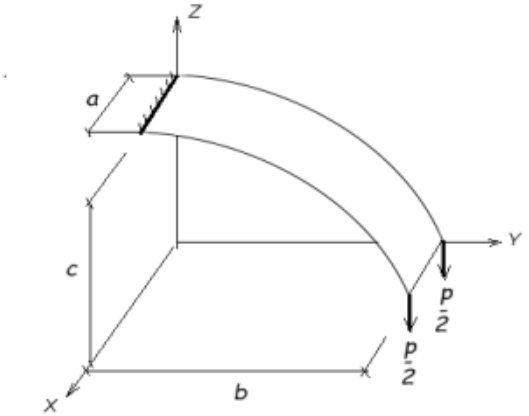

Fig. 1. Calculated structure

On the left edge, the structure is rigidly clamped. At the right edge, the shell is loaded with a tensile force of p = 160 N. The initial data were taken as follows: Young's modulus $E = 2 \cdot 10^6$ MPa, transverse strain coefficient μ = 0.32, structure thickness t = 0.5 cm. The yield strength was achieved at stress intensity and strain intensity: σ_{iT} = 200 MPa and ε_{iT} = 0.0023 MPa, respectively. Geometric design parameters: a = 1 cm, b = 10 cm, c = 5 cm.

An analysis of the finite element solutions obtained at the first loading step made it possible to establish the optimal number of discretization elements for further calculations of the structure under consideration. It was taken equal to 24.

Approximation of the deformation diagram for a nonlinear section in the presented example was carried out using the function

$$\sigma_i = A\varepsilon_i^2 + B\varepsilon_i + C \,. \quad (39)$$

where A = -23461.55 MPa, B = 181201.17 MPa, C = 1574.3 MPa.

The problem was solved in three different variants. In the first variant, the calculation was performed taking into account the hypothesis of the incompressibility of the material as a result of plastic deformations. To determine the dependencies between the first invariants of the strain and stress tensor, the coefficient $K_1 = \frac{1-2\mu}{E}$ was used. The numerical values of the stresses for this option are shown in Table 1. It presents the values of the hoop stresses σ_{22} on the left edge of the structure, depending on the coordinate ξ along the shell thickness and N number of loading steps.

Table 1. Values of hoop stresses in the implementation of the first variant of the defining equations

y coordinate, cm	ξ coordinate, cm	Stress, MPa		
		Number of loading steps, N		
		10	30	70
0.0	-0.25	-300.7	-309.0	-314.4
	-0.166	-259.0	-264.6	-266.2
	-0.083	-176.6	-188.5	-191.9
	0.0	-2.2	-2.8	-2.81
	0.083	172.0	182.9	186.2
	0.166	257.9	263.3	264.9
	0.25	299.6	307.6	310.1

In another variant of the calculation, the hypothesis of the incompressibility of the material was not taken into account and the relationship between the first invariants of the strain and stress tensor was carried out using the coefficient $K_2 = \frac{3}{2}\frac{(1-2\mu)}{(1+\mu)}\frac{1}{E_{sd}}$, obtained from the rod extension test. The numerical values of the hoop stresses for the second calculation variant are presented in Table 2.

The last variant of the calculation used the hypothesis of the proportionality of the components of the strain increment deviators and the components of the stress increment deviators (29). In this case, the dependencies between the first invariants of the strain and stress increment tensors were determined using the coefficient $K_3 = \frac{3}{2}\frac{(1-2\mu)}{(1+\mu)}\frac{1}{E_x}$. Table 3 shows the numerical values of the hoop stresses σ_{22} obtained in this variant of the shell calculation.

Table 2. Values of hoop stresses in the implementation of the second variant of the defining equations

y coordinate, cm	ξ coordinate, cm	Stress, MPa		
		Number of loading steps, *N*		
		10	30	70
0.0	-0.25	-291.1	-303.3	-306.6
	-0.166	-251.9	-261.1	-263.5
	-0.083	-184.7	-200.9	-205.4
	0.0	-2.6	-2.8	-2.89
	0.083	179.5	195.2	199.6
	0.166	250.7	259.8	262.3
	0.25	289.9	302.1	305.4

Table 3. Values of hoop stresses in the implementation of the third version of the defining equations

y coordinate, cm	ξ coordinate, cm	Stress, MPa		
		Number of loading steps, *N*		
		10	30	70
0.0	-0.25	-300	-308.8	-311.3
	-0.166	-258.8	-264.5	-266.2
	-0.083	-175.8	-188.6	-192.3
	0.0	-2.2	-2.7	-2.8
	0.083	171.4	183.1	186.4
	0.166	257.6	263.3	264.7
	0.25	299.9	307.8	310

In order to verify the computational process for the point of the left support section, diagrams of hoop stresses were constructed along the thickness of the structure. The number of steps, in this case, was taken equal to *N*=70. These diagrams for each of the calculation options are shown in Figs. 2-4.

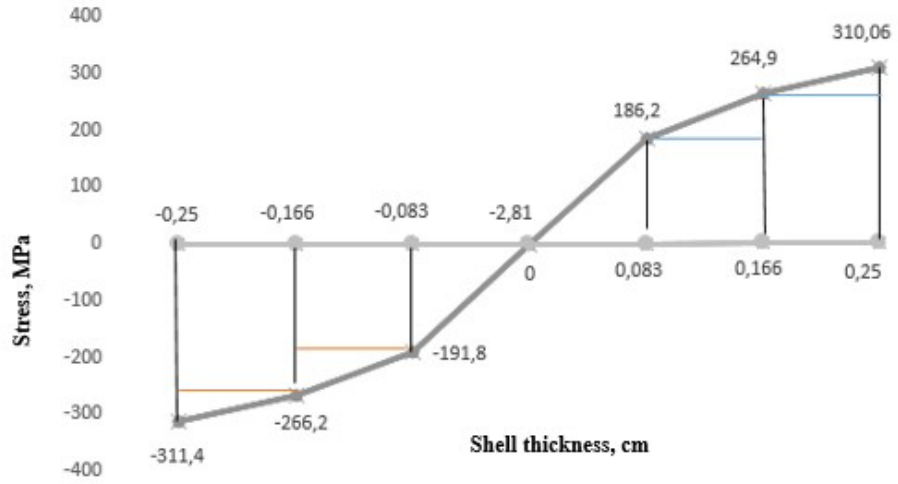

Fig. 2. Graph of stresses σ_{22} in the support section for the first calculation variant

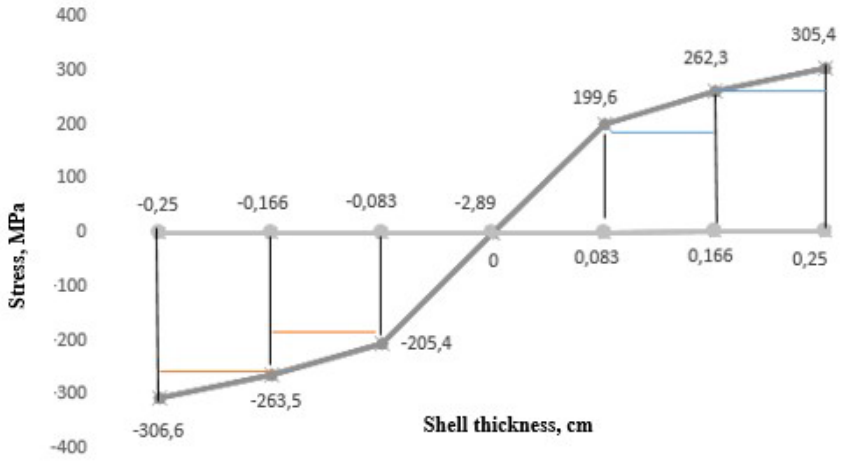

Fig.3. Graph of stresses σ_{22} in the support section for the second calculation variant

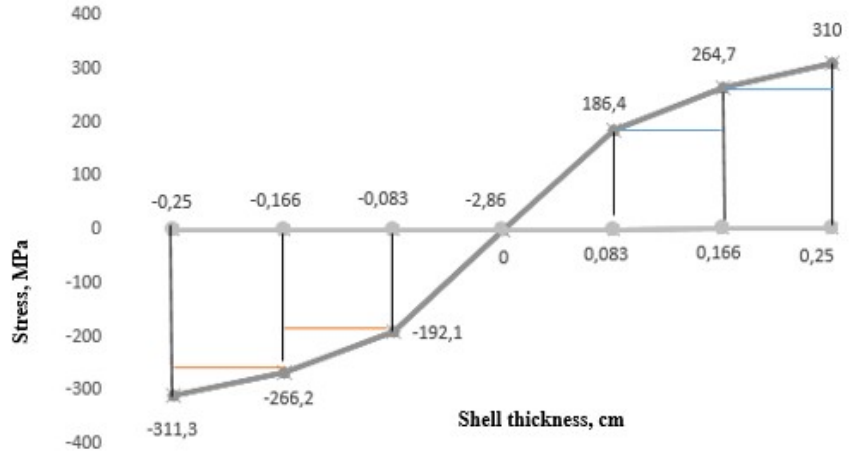

Fig. 4. Graph of stresses σ_{22} in the support section for the third calculation variant

4. Discussion

Verification of the computational process was carried out according to two main criteria. The numerical values of the hoop stress σ_{22} obtained for the considered point of the structure were compared with each other depending on the number of loading steps. With satisfactory convergence of the computational process, the pattern of the stress-strain state should not change significantly with an increase in the number of loading steps.

As can be seen from Tables 1-3, the convergence of the computational process in all the presented calculation options is satisfactory. The values of meridional stresses on the left edge of the shell with the number of steps N=10 and N=30 differ on average within 3%. With an increase in the number of steps to N=70, this difference decreases to 1%. The convergence condition is satisfied.

The second criterion for verifying the computational process is the ability to find the analytical value of the bending moment at the points of the support section and further compare them with the calculated variant indicators.

To determine the bending moment in the support section, the design scheme shown in Fig. 5 is used.

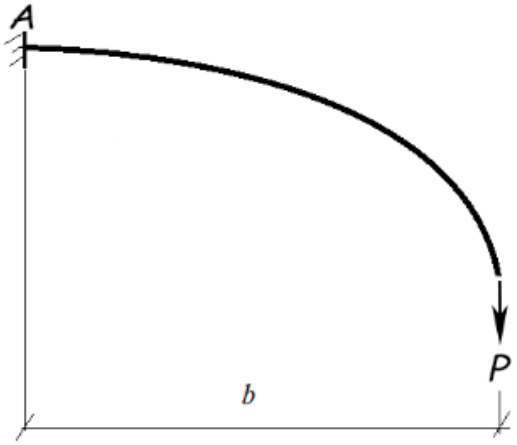

Fig. 5. Design scheme for determining the moment at point *A*

The numerical value of the bending moment at point *A* is

$$M_A = P \cdot b = 160 \cdot 10 = 1600\ H \cdot cm. \quad (40)$$

For each considered variant, the exact values of the bending moments on the left support edge of the shell were found. For this purpose, the corresponding diagram of meridional stresses was divided into simple geometric figures and their areas were calculated. The calculated forces were multiplied by the corresponding shoulders, equal to the distance from the center of gravity of the elementary geometric figure to the middle surface. The sum of all calculated products is equal to the total bending moment.

Taking into account the hypothesis of material incompressibility as a result of plastic deformations (variant 1), the total bending moment at point *A* was $M_1 = 1582.7$ N·cm, for the second variant M_2 = 1576.2 N·cm, and in the third calculation variant, this value was equal to M_3 = 1583.4 N·cm. The errors in calculating the moments compared with the result (40) turned out to be equal to $\delta_1 = 1.08\%$, $\delta_2 = 1.48\%$, and $\delta_3 = 1.03\%$ for each of the variants, respectively.

5. Conclusions

The analysis of the presented material allows us to draw the following conclusions. The developed algorithm for taking into account physical nonlinearity makes it possible to obtain reliable finite element solutions in the calculations of arbitrary shell structures, the middle surface of which can be described by equation (1).

In the example of a test problem, numerical values of circumferential stresses satisfactory for computational engineering practice were obtained for various variants of defining equations. The calculation errors do not exceed 2%.

The use of the classical assumption that there is no change in volume as a result of plastic deformations is, according to the authors, not sufficiently correct. The relationship between the average linear strain and the average linear stress at the loading step, as shown by the calculation result, is best calculated using (25). This more fully corresponds to the physical meaning of the deformation process.

Based on the results obtained in the third variant of the calculation, we can conclude that the defining relations without separation into the elastic and plastic parts of the deformations at the loading step, found using the hypothesis of the proportionality of the components of the deviators of the increments of deformations and the components of the deviators of the increments of stresses, are more consistent with the physical meaning of the deformation process. In addition, the implementation of this hypothesis makes it possible to significantly simplify the procedure for forming the plasticity matrix at the loading step, since it eliminates the need to differentiate strains with respect to stresses.

References

[1] Krivoshapko SN. On opportunity of shell structures in modern architecture and building. *Structural Mechanics of Engineering Constructions and Buildings.* 2013;1: 51-56.
[2] Reissner E. Linear and Nonlinear Theory of Shells. Thin-shell structures: theory, experiment and Design. In: *Prentice.* Hall inc.; 1974. p.29-44
[3] Levin VA, Vershinin AV. *Numerical methods*. Moscow: Fizmatlit; 2015. (In Russian)
[4] Levin VA. *Models and methods*. Moscow: Fizmatlit; 2015. (In Russian)
[5] Kayumov RA. Postbuckling behavior of compressed rods in an elastic medium. *Mechanics of Solids*. 2017;52(5): 575-580.
[6] Aldakheei F, Wriggers P, Miehe C. A modified Gurson-type plasticity model at finite strains: formulation, numerical analysis and phase-field coupling. *Computational Mechanics*. 2018;62: 815-833.
[7] Aldakheev F, Miehe C. Coupled thermomechanical response of gradient plasticity. *International Journal of Plasticity*. 2017;91: 1-24.
[8] Aldakheel F. Micromorphic approach for gradient-extended thermo-elastic-plastic solids in the algorithmic strain space. *Continuum Mechanics Thermodynamics.* 2017;29(6): 1207-1217.
[9] Sultanov LU. Analysis of finite elasto-plastic strains. Medium kinematics and constitutive equations. *Lobachevskii Journal of Mathematics*. 2016;37(6); 787-793.
[10] Wriggers P, Hudobivnik B. A low order virtual element formulation for finite elastoplastic deformations. *Computer Methods in Applied Mechanics and Engineering*. 2017;2: 123-134.
[11] Artioli E, Beirao da Veiga L, Lovadina C, Sacco E. Arbitrary order 2D virtual elements for polygonal meshes: Part II, inelastic problem. *Computational Mechanics*. 2017;60: 643-657.
[12] Beirao Da Veiga L, Lovadina C, Mora D. A virtual element method for elastic and inelastic problems on polytope meshes. *Computer Methods in Applied Mechanics and Engineering.* 2017;295: 327-346.
[13] Hudobivnik B, Aldakheel F, Wriggers P. A Low order 3D Virtual element formulation for finite elasto-plastic deformations. *Computational Mechanics*. 2019;63: 253-269.
[14] Pi YL, Bradford MA, Tin-Loi F. Non-linear in-plane buckling of rotationally restrained shallow arches under a central concentrated load. *International Journal of Nonlinear Mechanics.* 2008;43: 1-17.
[15] Tupyshkin ND, Zapara MA. Opredelyayushchiye sootnosheniya tenzornoy teorii plasticheskoy povrezhdayemosti metallov. In: *Problemy prochnosti, plastichnosti i ustoychivosti v mekhanike deformiruyemogo tverdogo tela*. Tver: Izd-voTvGTU; 2011. p.216-219. (In Russian)
[16] Lalin V, Rybakov V, Sergey A. The finite elements for design of frame of thin-walled beams. *Applied Mechanics and materials*. 2014;578-579: 858-863.
[17] Yefanov KV. Raschet neftyanykh apparatov metodom konechnykh elementov. *Litres*: Samizdat.; 2020. (In Russian)
[18] Badriev IB, Paimushin VN. Refined models of contact interaction of a thin plate with postioned on both sides deformable foundations. *Lobachevskii Journal of Mathematics*. 2017;38(5): 779-793.
[19] Krysl P. Mean-strain 8-node hexahedron with optimized energy-sampling stabilization. *Finite elements in Analysis and Design*. 2016;108: 41-53.
[20] Liang K, Ruess M, Abdalla M. Co-rotational finite element formulation used in the Koiter-Newton method for nonlinear buckling analyses. *Finite elements in Analysis and Design*. 2016;116: 38-54.

[21] Magisano D, Leonetti L, Garcea G. Advantages of mixed format in geometrically nonlinear of beams and shells using solid finite elements. *International Journal for Numerikal Methods Engineering*. 2017;109(9): 1237-1262.
[22] Aldakheel F, Hudobivnik B, Wriggers P. Virtual element formulation for phase-field modeling of ductile fracture. *International Journal for Multiscale Computational Engineering*. 2019;17(2): 181-200.
[23] Magisano D, Leonetti L, Garcea G. Koiter asymptotic analysis of multilayered composite structures using mixed solid-shell finite elements. *Composite Structures*. 2016;154: 296-308.
[24] Chi H, Talischi C, Lopez-Pamies O, Paulino GH. Polygonal finite elements for finite elasticity. *International Journal for Numerical Methods in Engineering*. 2015;101: 305-328.
[25] Tyukalov YY. Equilibrium finite elements for plane problems of the elasticity theory. *Magazine of Civil Engineering*. 2019;91(7): 80-97.
[26] Gureyeva NA, Klochkov YV, Nikolayev AP, Klochkov MY. Nepreryvnaya parametrizatsiya sredinnoy poverkhnosti ellipsoidalnoy obolochki i yeye geometricheskiye parametry. *Matematicheskaya fizika i kompyuternoye modelirovaniye*. 2020;23(1): 5-12.
[27] Sedov LI. *Continuum Mechanics.* Moscow: Science; 1976. (In Russian)
[28] Dzhabrailov AS, Klochkov YV, Nikolayev AP, Fomin SD. Opredeleniye napryazheniy v obolochkakh vrashcheniya pri nalichii zon sochleneniya na osnove treugolnogo konechnogo elementa s uchetom uprugoplasticheskogo deformirovaniya. *Izvestiya vysshikh uchebnykh zavedeniy. Aviatsionnaya tekhnika*. 2015;1: 8-13. (In Russian)
[29] A.A. Ilyushin. *Plastichnost*. *Uprugo-plasticheskiye deformatsii*. S-Peterburg*:* Lenand; 2018. (In Russian)
[30] Malinin MM. *Applied Theory of Plasticity and Creep*. Moscow: Engineering; 1975.

THE AUTHORS

Dzhabrailov A.Sh.
e-mail: arsen82@yandex.ru
ORCID: 0000-0001-6494-1377

Nikolaev A.P.
e-mail: anpetr40@yandex.ru
ORCID: 0000-0002-7098-5998

Klochkov Yu.V.
e-mail: klotchkov@bk.ru
ORCID: 0000-0002-1027-1811

Gureyeva N.A.
e-mail: natalya-gureeva@yandex.ru
ORCID: 0000-0003-3496-2008